https://ntrs.nasa.gov/search.jsp?R=19890011733 2020-03-20T02:35:17+00:00Z

NASA Technical Memorandum 101971

Simulation of the Low Earth Orbital Atomic Oxygen Interaction With Materials by Means of an Oxygen Ion Beam

Bruce A. Banks and Sharon K. Rutledge
National Aeronautics and Space Administration
Lewis Research Center
Cleveland, Ohio

Phillip E. Paulsen
Cleveland State University
Cleveland, Ohio

and

Thomas J. Steuber
Sverdrup Technology, Inc.
NASA Lewis Research Center Group
Cleveland, Ohio

Prepared for the
18th Annual Symposium on Applied Vacuum Science and Technology
sponsored by the American Vacuum Society
Clearwater Beach, Florida, February 6–8, 1989

NASA

(NASA-TM-101971) SIMULATION OF THE LOW EARTH ORBITAL ATOMIC OXYGEN INTERACTION WITH MATERIALS BY MEANS OF AN OXYGEN ION BEAM (NASA) 32 p
CSCL 11C
N89-21104
Unclas
G3/27 0200245

SIMULATION OF THE LOW-EARTH ORBITAL ATOMIC OXYGEN INTERACTION WITH MATERIALS BY MEANS OF AN OXYGEN ION BEAM

Bruce A. Banks and Sharon K. Rutledge
National Aeronautics and Space Administration
Lewis Research Center
Cleveland, Ohio 44135

Phillip E. Paulsen
Cleveland State University
Department of Electrical Engineering
Cleveland, Ohio 44115

and

Thomas J. Stueber
Sverdrup Technology, Inc.
NASA Lewis Research Center Group
Cleveland, Ohio 44135

SUMMARY

Atomic oxygen is the predominant species in low-Earth orbit between the altitudes of 180 and 650 km. These highly reactive atoms are a result of photodissociation of diatomic oxygen molecules from solar photons having a wavelength less than or equal to 2430 Å. Spacecraft in low-Earth orbit collide with atomic oxygen in the 3P ground state at impact energies of approximately 4.2 to 4.5 eV. As a consequence, organic materials previously used for high altitude geosynchronous spacecraft are severely oxidized in the low-Earth orbital environment. The evaluation of materials durability to atomic oxygen requires ground simulation of this environment to cost effectively screen materials for durability. Directed broad beam oxygen sources are necessary to evaluate potential spacecraft materials performance before and after exposure to the simulated low-Earth orbital environment. This paper presents a description of a low energy, broad oxygen ion beam source used to simulate the low-Earth orbital atomic oxygen environment. The results of materials interaction with this beam and comparison with actual in-space tests of the same materials will be discussed. Resulting surface morphologies appear to closely replicate those observed in space tests.

E-4671

INTRODUCTION

Background

The effects of low-Earth orbital (LEO) atomic oxygen interaction with various materials have been studied on space shuttle flights over the past several years (ref. 1). The results of these tests indicate the existence of three major categories of materials evaluated in LEO: (1) materials which readily oxidize, such as most organic polymers; (2) materials which are not readily oxidized or form protective oxide barriers to inhibit further oxidation, such

as most metals; and (3) materials which form volatile oxides at a slow but non-zero rate, such as fluoropolymers. Quantification of the susceptibility of a material to atomic oxygen attack is described as an erosion yield, which is the ratio of the volume or mass of material loss per each incident oxygen atom. The volume erosion yields of over 60 materials evaluated in various low-Earth orbital space experiments are presented in table I.

Many factors may influence the erosion yield of materials, such as impact angle, material temperature, atomic oxygen flux, atomic oxygen fluence, synergistic solar radiation, and atomic oxygen impact energy. Because of the limited amount of in-space testing performed to date, the degree to which these factors influence erosion yield is not well understood. All materials which form volatile oxides upon atomic oxygen bombardment have been found to develop a microscopic surface texture composed of left-standing fibrils or cones. This texture tends to have an influence on the optical properties of materials, causing a significant increase in diffuse reflectance. Table II delineates the changes in solar absorptance and thermal emittance of materials exposed to low-Earth orbital atomic oxygen.

Knowledge of the long-term durability of materials exposed to low-Earth orbital atomic oxygen is crucial to numerous space missions and experiments, such as those being planned in conjunction with Space Station Freedom. Because of the costs associated with in-space performance characterization of candidate materials, ground-based laboratory facilities which simulate the effects of atomic oxygen interaction with materials in low-Earth orbit are desirable. The low-Earth orbital atomic oxygen environment is particularly difficult to simulate because oxygen is essentially in the 3P ground state with mean energies between 4.2 and 4.5 eV. It is very difficult to obtain neutral atomic species at energies which are high compared to convenient thermal energies and low compared to convenient electrostatic energies. As a result, it has been difficult to construct reliable, energetic neutral atom, broad beam facilities with adequate flux to enable accelerated testing of materials. Figure 1 depicts many of the current processes used to simulate the effects of low-Earth orbital atomic oxygen attack on materials. Figure 2 is a flux energy domain plot for 32 atomic oxygen test facilities participating in the NASA Atomic Oxygen Effects Test Program. This test program is intended to further the understanding of atomic oxygen mechanisms and simulation phenomena through collective information gathered from numerous simulation facilities and space test results (ref. 2). The facility numbers shown in figure 2 correspond to the facility numbers and descriptions listed in table III.

Need for Broad Oxygen Beam Exposure Capability

The least expensive and most convenient technique used for evaluating the susceptibility of materials to atomic oxygen attack involves the use of radio frequency oxygen plasma dischargers, commonly called plasma ashers. As can be seen in figure 2, plasma ashers typically produce atomic oxygen at thermal energies of a fraction of an electronvolt. These devices, which also produce excited state species as well as ions and neutral species, are the most commonly used devices for screening material durability to atomic oxygen. Although the energy and purity of species are not optimal, materials which are oxidized by atomic oxygen in plasma ashers have generally been found to oxidize in low-Earth orbit, and materials which have demonstrated atomic oxygen

durability in plasma ashers have been found to be durable in low-Earth orbit. However, there are complications associated with using erosion yield results from plasma ashers to predict performance in space. The relative ranking of erosion rates of a wide variety of materials from asher data frequently does not prove to be reliable for predicting in-space results.

Some materials of mixed organic and inorganic composition indicate modes of oxidative failure in plasma asher testing which may not occur in space. Figure 3 shows a scanning electron photomicrograph of a graphite-epoxy composite sample which was coated with a mica-filled paint and then exposed to atomic oxygen in an RF plasma asher (ref. 3). After exposure, microscopic flakes of mica completely covered the entire exposed surface of the sample, with no paint vehicle remaining. When the flakes were removed, it was quite apparent that atomic oxygen had oxidized the graphite-epoxy surface in spite of the physical appearance of a protective layer. This oxidation may have been produced by RF exitation of gas trapped in voids underneath the protective covering or perhaps by scattering of atomic oxygen which impacted the protective surface from all directions rather than unidirectionally.

Figure 4 shows a photograph of fiberglass-epoxy composite samples before and after exposure to atomic oxygen in an RF plasma asher (ref. 4). When oxidation of the epoxy occurs, the friable glass fibers free themselves from attachment to the underlying bulk material. This process would be expected to slowly terminate because of the glass fibers eventually shielding the underlying epoxy from atomic oxygen attack. However, as can be seen in figure 5, although the rate of mass loss is reduced when the fibers are exposed at an equivalent fluence based on Kapton of approximately 2×10^{21} atoms/cm^2, no further evidence of self-shielding or protection occurs, and the mass loss per unit area continues without any reduction in rate. Somehow, in the RF plasma asher, atomic oxygen is presenting itself to the underlying epoxy without increasing obstruction from the overlying glass fiber layer. In space, the directed atomic oxygen would be expected to gradually be prevented from attacking the underlying epoxy. This may not occur in RF plasma ashers if exitation of the voids between the glass fibers occurs such that exposed glass fibers do not contribute to the protection of the underlying epoxy.

Many high performance materials being considered for use in the low-Earth orbital environment, such as graphite-epoxy or polyimide Kapton, will require atomic oxygen protective coatings. The functional life of these protective coatings depends, to a large degree, upon atomic oxygen interaction at sites of defects in the coatings. In space, atomic oxygen will attack the oxidizable organic material beneath a defect, but the degree of undercutting may be substantially reduced from that obtained in RF plasma ashers because of higher energy and more directed arrival, as illustrated in figure 6. Later in this paper, it will be shown that atomic oxygen has a higher probability of interacting if it has higher impact energy. The lower energy atomic oxygen in plasma ashers arrives at all angles, inviting undercutting, and has a higher probability of scattering and reduced probability of interacting on first impact, which may contribute to undercutting.

Because protective coatings for organic materials must be evaluated for durability in ground simulation systems, it is essential that directed oxygen beam systems be free from these types of flaws, which may cause one to arrive at incorrect conclusions about the modes of failure and lifetime of materials

in low-Earth orbit. It is also desirable for a directed oxygen beam system to have a beam area of an adequate size to perform optical and mechanical functional performance evaluation of candidate materials (typically several centimeters in diameter).

Ion Versus Neutral Atom Considerations

The low-Earth orbital atomic oxygen simulation technique described in this paper utilizes an oxygen ion beam to simulate the effects of neutral atomic oxygen. An unneutralized ion beam impacting an insulating surface will quickly charge the surface to a high positive potential, thus preventing the arrival of additional ions unless that ion beam is space charge neutralized. The ion beam system described in this paper is space charge neutralized by means of an electron emitting filament. Although the electrons do not microscopically reassociate with each ion, they do maintain space charge neutrality and are available to prevent surface charging of insulators.

When ions impact a surface, an electron image charge is present on that surface as the ion approaches impact. Prior to impact, the high electric fields associated with the ion-electron image pair cause the electron to be extracted from the surface and neutralize the incoming ion (ref. 5). Although the oxygen ion now impacts the surface as a neutral atom, there are two issues which may play a role in the impact chemistry which occurs. The incoming atom may be excited by gaining energy in the neutralization process equal to the ionization energy. Also, since the surface has lost an electron, this local charge may contribute to chemical decomposition processes in some materials.

OXYGEN ION BEAM SYSTEM

Vacuum Facility

The oxygen ion beam system is operated in a vacuum facility which is 71 cm in diameter and 171 cm long. The vacuum facility shown in figure 7 is pumped by a perfluorinated ether (Fomblin) diffusion pump oil and roughing pump oil. Figure 8 shows a schematic of the ion beam vacuum system. The vacuum facility is capable of maintaining a pressure of 10^{-4} torr during ion beam source operation with an input source gas flow of 20 standard cubic centimeters/minute of oxygen.

Ion Source

To obtain an adequate flux of ions at low energies, it was necessary to utilize a gridless (end Hall) ion source (ref. 6). The ion source uses a single thermionic cathode as an electron emitter to ionize oxygen gas molecules. The cathode is a source of electrons for space charge neutralization as well. A plasma is formed in the presence of an axially diverging magnetic field, and O_2^+ and O^+ ions are formed and accelerated to the order of tens of electron-volts and allowed to impinge on samples located downstream of the ion source. Figure 9 shows a schematic of the gridless ion source. To maintain acceptable sample temperatures at high ion fluxes, it was found to be necessary to shield radiant energy of the cathode from illuminating samples placed downstream of

the ion source. Use of the cathode filament radiation shield reduces the sample temperature while still allowing exposure of samples up to 10 cm in diameter. This area is large enough to perform thermal emittance, solar absorptance, and mechanical characterization of materials exposed to the directed oxygen beam. Figure 10 shows photographs of the ion source relative to the sample holder plate, which contains a current density probe and a quartz crystal microbalance. The sample holder plate is water cooled to maintain acceptable sample temperatures for heat sensitive polymeric samples. Figure 11 shows the dependence of ion energy as a function of applied discharge voltage in the ion source (ref. 6). The gridless ion source produces a divergent ion beam as can be seen in the current density profiles at various locations downstream shown in figure 12. Each milliamp per square centimeter of oxygen ion beam arrival current density represents between 6.25×10^{15} and 1.25×10^{16} oxygen atoms/square centimeter, depending on the ratio of O^+ to O_2^+ in the ion beam.

RESULTS AND DISCUSSION

Current Density

Measured current densities as a function of anode potential, oxygen flow rate, and axial distance downstream of the ion source are shown in figures 13(a), (b), and (c), respectively. As can be seen in figure 13(c), for sample target locations 59 cm downstream of the ion source, ion current densities of 0.16 mA/cm^2 are typically achieved. This represents an atomic oxygen flux of 1×10^{15} atoms/cm^2/sec, assuming the beam is 100 percent O^+; or 2×10^{15} atoms/cm^2/sec, assuming the oxygen ion beam is 100 percent O_2^+. Although characterization of monatomic to diatomic oxygen ion content is planned at the present time, without this information, the oxygen flux can only be specified to within a factor of 2.

Target Temperatures

Use of a radiation shield downstream of the cathode filament reduced sample temperatures from greater than 204 °C to less than 41 °C at sample to ion source distances of 20 cm, based on readings obtained from temperature sensing indicator strips placed on samples located downstream of the ion source.

Erosion Yields of Materials

The erosion yields of five materials selected for the NASA Atomic Oxygen Effects Test Program were evaluated in this ion beam facility. These materials include Kapton HN polyimide, low oxygen content polyethylene, FEP Teflon, pyrolytic graphite, and highly oriented pyrolytic graphite (ref. 2). Table IV compares the erosion yields of these materials with similar materials tested in space. As can be seen in table IV, erosion yields resulting from the ion beam tests are significantly higher than those observed from in-space testing. This is not surprising, because the energy of the oxygen ions is an order of magnitude higher than the energy of atomic oxygen in low-earth orbit. Figure 14 shows a plot of the erosion yield of polyimide Kapton as a function of oxygen ion or atom energy (ref. 7). A wide range of oxygen ion or atom energies is shown on this plot, including data from the facility described in this paper.

Over a large range of energy, the erosion yield appears to depend on the 0.68 power of the oxygen atom or ion energy (ref. 7). Based on this erosion yield versus energy dependence, the ground laboratory oxygen ion beam data for Kapton HN presented in table IV would be expected to produce an erosion yield of 3×10^{-23} cm^3 per atom, or a factor of 4.7 higher erosion yield, because the oxygen ions had an energy of 41 eV rather than 4.2 to 4.5 eV, which occurs in low-Earth orbit. It is also interesting to note that, although the erosion yields of polyethylene and graphite also appear to be increased by an order of magnitude as a result of this higher energy, the erosion yield of FEP Teflon was increased by 10^3. This may be a consequence of the individual materials' erosion yield dependence upon energy; or it may be a result of differences between ground laboratory ion exposure and in-space exposure, such as synergistic UV exposure effects or phenomena associated with the ion beam as opposed to a neutral atom beam. Figure 15 shows a photograph of these five materials before and after ion beam exposure to a fluence of 7×10^{18} to 1.5×10^{19} atoms/cm^2. Figure 16 shows the typical increase in diffuse reflectance of polyimide Kapton exposed to the oxygen ion beam. Figures 17(a) and (b) show scanning electron photomicrographs of the surface of samples of polyimide Kapton HN and pyrolytic graphite exposed to an oxygen beam at a fluence of 3×10^{19} to 6×10^{19} and 8×10^{19} to 1.6×10^{20} atoms/cm^2, respectively. These microscopic surface structures appear similar to those which have been observed in space.

Chemical Reactions versus Physical Sputtering

As the energy of oxygen atoms or ions is increased from the thermal energies of an asher to the high energies of several hundred electronvolt ions, the mechanisms for removal of target materials may change from directed chemical oxidation and volatilization to physical sputtering. Although the sputtering threshold of most materials is of the order of tens of electronvolts, physical sputtering of oxygen does not appear to be a dominant surface recession mechanism until one achieves energies on the order of 100 eV. Figure 18 shows the sputter yield for oxygen ions on nickel as a function of energy (ref. 8). The oxygen ion energy in low-Earth orbital simulation systems must be sufficiently low so that physical sputtering of thin film atomic oxygen protective coatings occurs at a very slow rate. Chemical atomic oxygen attack rather than physical sputtering must be the dominant degradation mechanism to properly assess materials durability in low-Earth orbit.

SUMMARY OF RESULTS

Although numerous materials have been evaluated in space, schemes for protection of materials which might oxidize in space have not been fully demonstrated in space and must be evaluated in ground-based laboratory tests prior to consideration for in-space testing. An oxygen ion beam can be used to simulate the effects of low-Earth orbital atomic oxygen attack on materials. The reactivity of the oxygen ion beam appears to be higher than that observed in space. This may be partially due to the higher energy which contributes to the reactivity. The microscopic surface textures produced by oxygen ion beam simulation appear to closely replicate those observed in space. Use of a gridless ion source in conjunction with a cathode filament radiation shield allows the exposure of heat sensitive polymeric materials without thermal decomposition problems. Samples up to 10 cm in diameter can be exposed, allowing post-exposure optical and mechanical characterization of materials to be performed.

The oxygen ion energies appear to be sufficiently low so that chemical reaction and not physical sputtering is the dominant mechanism of material removal.

REFERENCES

1. B.A. Banks and S.K. Rutledge, Low Earth Orbital Atomic Oxygen Simulation for Materials Durability Evaluation. Presented at the 4th International Symposium on Spacecraft Materials in Space Environment, Toulouse, France, Sept. 6-9, 1988. (To be published by European Space Agency.)

2. B.A. Banks, S.K. Rutledge, and J.A. Brady, in Fifteenth Space Simulation Conference: Support the Highway to Space Through Testing, J. Stecher, ed., NASA CP-3015, (NASA, Washington, D.C., 1988), pp. 51-65.

3. S.K. Rutledge, B.A. Banks, F. DiFilippo, J.A. Brady, T. Dever, and D. Hotes, "An Evaluation of Candidate Oxidation Resistant Materials for Space Applications in LEO." NASA TM-100122, 1986.

4. S.K. Rutledge, P.E. Paulsen, J.A. Brady, and M.L. Ciancone, "Oxidation and Protection of Fiberglass-Epoxy Composite Masts for Photovoltaic Arrays in the Low Earth Orbital Environment," NASA TM-100839, 1988.

5. H.D. Hagstrum, in Inelastic Ion-Surface Collisions; N.H. Tolk, J.C. Tully, W. Heiland, and C.W. Tully, eds., (Academic Press, New York, 1977), pp. 1-25.

6. H.R. Kaufman, R.S. Robinson, and W.E. Hughes, "Characteristics, Capabilities, and Applications of Broad-Beam Sources." Commonwealth Scientific Corporation, Ft. Collins, CO, 1987.

7. D.C. Ferguson, in Thirteenth Space Simulation Conference, J. Stecher, ed., NASA CP-2340, (NASA, Washington, D.C., 1984), pp. 205-221.

8. H.L. Bay, J. Bohdansky, and E. Hechtl, Radiation Effects, 41, 77 (1979).

TABLE I. - EROSION YIELDS OF VARIOUS MATERIALS EXPOSED TO ATOMIC OXYGEN IN LOW-EARTH ORBIT

Material	Erosion yield, $\times 10^{-24}$ cm^3/atom	Reference
Aluminum (150 Å)	0.0	1
Aluminum-coated Kapton	.01	2
Aluminum-coated Kapton	.1	2
Al_2O_3	<.025	3
Al_2O_3 (700 Å) on Kapton H	<.02	4
Apiezon grease 2 mm	>.625	5
Aquadag E (graphite in an aqueous binder)	1.23	6
Carbon	1.2	7, 1, 8, 9
Carbon (various forms)	.9 to 1.7	10
Carbon/Kapton 100XAC37	1.5	11
401-C10 (flat black)	.30	12
Chromium (123 Å)	Partially eroded	14
Chromium (125 Å) on Kapton H	.006	15, 16
Copper (bulk)	0.0	17
Copper (1000 Å) on sapphire	.007	15, 16
Copper (1000 Å)	.0064	14
Diamond	.021	17
Electrodag 402 (silver in a silicone binder)	.057	6
Electrodag 106 (graphite in an epoxy binder)	1.17	6
Epoxy	1.7	10, 16
Fluoropolymers:		
FEP Kapton	.03	18
Kapton F	<.05	6
Teflon, FEP	.037	5
Teflon, FEP	<.05	10
Teflon, TFE	<.05	10, 6
Teflon, FEP and TFE	0.0 and 0.2	15, 19
Teflon, FEP and TFE	.1	15
Teflon	.109	18
Teflon	.5	15
Teflon	.03	15
Teflon	<.03	9
Gold (bulk)	0.0	17
Gold	Appears resistant	20
Graphite epoxy:		
1034 C	2.1	10
528/T300	2.6	10
GSFC green	0.0	1
HOS-875 (bare and preox)	0.0	1, 26
Indium Tin oxide	.002	15, 16
Indium Tin oxide/Kapton (aluminized)	.01	2
Iridium film	.0007	17
Lead	0.0	1, 26
Magnesium	0.0	1, 26
Magnesium fluoride on glass	.0007	15, 16
Molybdenum (1000 Å)	.0056	4
Molybdenum (1000 Å)	.006	15, 16
Molybdenum	0.0	1, 26
Mylar	3.4	10
Mylar	2.3	15, 19
Mylar	3.9	15, 19, 9
Mylar	1.5 to 3.9	15
Mylar A	3.7	18
Mylar A	3.4	21, 6
Mylar A	3.6	6
Mylar D	3.0	6
Mylar D	2.9	21
Mylar with Antiox	Heavily attacked	22

TABLE I. - Continued.

Material	Erosion yield, $\times 10^{-24}$ cm^3/atom	Reference
Nichrome (100 Å)	0.0	1
Nickel film	0.0	17
Nickel	0.0	8, 26
Niobium film	0.0	17, 1
Osmium	.026	10
Osmium	Heavily attacked	20
Osmium (bulk)	.314	17
Parylene, 2.5 mm	Eroded away	22
Platinum	0.0	1, 26
Platinum	Appears resistant	20
Platinum film	0.0	17
Polybenzimidazole	1.5	10, 7
Polycarbonate	6.0	8
Polycarbonate resin	2.9	17
Polyester - 7% Polysilane/93% Polyimide	.6	10
Polyester	Heavily attacked	10, 22
Polyester with Antiox	Heavily attacked	10, 22
Polyester (Pen-2,6)	2.9	23
Polyethylene	3.7	10, 21, 16, 15
Polyethylene	3.3	18, 6
Polyimides:		
BJPIPSX-9	.28	23
BJPIPSX-9	.071	24
BJPIPSX-11	.56	23
BJPIPSX-11	.15	24
BTDA-Benzidene	3.08	23
BTDA-DAF	2.82	23
BTDA-DAF	.08	24
BTDA-mm-DDS02	2.29	23
BTDA-mm-MDA	3.12	23
BTDA-pp-DABP	2.91	23
BTDA-pp-ODA	3.97	23
I-DAB	1.80	23
Kapton (black)	1.4 to 2.2	15, 12
Kapton (TV blanket)	2.0	15
Kapton (TV blanket)	2.04	19
Kapton (OSS - 1 blanket)	2.55	15
Kapton (OSS - 1 blanket)	2.5	15
Kapton H	3.0	10, 15, 19, 4, 6, 9
Kapton H	2.4	15, 19
Kapton H	2.7	15, 18
Kapton H	1.5 to 2.8	15
Kapton H	2.0	18
Kapton H	3.1	18
Kapton (uncoated)	.1 and .06	2
ODPA-mm-DABP	3.53	23
PEN-2.6	2.90	23
PMDA-pp-DABP	3.82	23
PMDA-pp-MDA	3.17	23, 24
PMDA-pp-ODA	4.66	23
Polymethylmethacrylate	3.1	16
7% Polysilane/93% Polyimide	.6	10
25% Polysiloxane, 75% Polyimide	.3	10
25% Polysiloxane	.3	9
Polystyrene-Polyimide	1.7	10, 16, 9
Polysulfone	2.4	10, 16
Polyvinylidene fluoride	0.6	9
Pyrone: PMDA-DAB	2.5	23

TABLE I. - Concluded.

Material	Erosion yield, $\times 10^{-24}$ cm^3/atom	Reference
S-13-GLO, white	0.0	12
SiO_2 (650 Å) on Kapton H	<.0008	4
SiO_2 (650 Å) with ≤4% PTFE	<.0008	4
SiOx/Kapton (aluminized)	.01	2
Silicones:		
DC1-2577	.055	21
DC1-2755-coated Kapton	.05	15
DC1-2775-coated Kapton	<.5	15
DC6-1104	.0515	20
Grease 60 mm	Intact but oxidized	25
RTV-560	.443	21
RTV-615 (black, conductive)	0.0	20
RTV-615 (clear)	.0625	5
RTV-670	0.0	1
RTV-S695	1.48	11
RTV-3145	.128	1
T-650-coated Kapton	<.5	15
Siloxane polyimide (25% Sx)	.3	7
Siloxane polyimide (7% Sx)	.6	7
Silver	10.5	5
Tantalum	Appears resistant	20
Tedlar	3.2	10
Tedlar (clear)	1.3 and 3.2	15
Tedlar (clear)	3.2	18, 6
Tedlar (white)	.4 and .6	15
Tedlar (white	.05	15
TiO_2, (1000 Å)	.0067	5
Trophet 30 (bare and preox)	0.0	1, 26
Tungsten	0.0	8, 26
Tungsten carbide	0.0	8
YB-71 (ZOT)	0.0	7
Z302 (glossy black)	3.9	26

TABLE II. - EFFECT OF LEO ATOMIC OXYGEN ON OPTICAL PROPERTIES OF MATERIALS

Material	Change in optical properties due to atomic oxygen			Reference
	Solar absorptance	Emittance	Reflectance	
Ag/FEP	0.006	0.0	------	I
Al/Al_2O_3	-.006	0.0	------	I
$AlMgF_2$	-----	-----	0.0	B
Al_2O_3	0.0	-----	0.0	E
Al_2O_3/Al(He)	-.005	0.0	------	I
Al_2O_3/Al(Le)	-.006	0.0	------	I
Aluminized FEP Teflon, second surface mirror (0.025 mm thick)	.05	-.19	------	O
Al Kapton	.048	.018	------	K
Al Kapton	-.062	-.007	------	K
Aluminized Kapton, second surface mirror, uncoated (0.052 mm thick)	-.23	-.59	------	O
Aluminum (150 Å)	0.0	0.0	0.0	B
Aluminum (chromic acid oxidized)	0.0	0.0	0.0	F
Black, carbon-filled PTEE impregnated fiberglass (0.127 mm thick)	-.16	-.05	------	O
Black Cr on Cr on Mo	-----	-----	[a].20	N
Black Ir on Mo	-----	-----	-.75	N
Black Rh on Mo (matte)	-----	-----	-.25	N
Black Rh on Mo (specular)	-----	-----	-.50	N
Bostic 463-14	.01	0.0	------	J
Chemglaze A276 (w/modifiers)	.006 to .016	.02	------	A
Chemglaze A276 (white)	.005	.03	-.039	B,C
Chemglaze Z004	.01	0.0	------	J
Chemglaze Z302 (glossy, black)	.011	-----	-.01	D
Chromium (123 Å)	0.0	0.0	0.0	E
FEP Teflon with silver undercoat	.006	0.0	------	---
GE-PD-224	0.0	0.0	------	J
GSFC (green)	-.002	-----	------	L
Indium tin oxide coated Kapton H with aluminized backing	.006	.004	------	K
ITO ring	.006	.004	------	K
ITO (S) Sheldahl, black/ Kapton (sputtered)	.01	0.0	------	J
ITO (VD) Sheldahl, black/ Kapton (vacuum deposited)	0.0	0.0	------	J
Ir foil on Al	-----	-----	0.0	N
KAT glass	-----	-----	[b]-.051 to .01	N
Kapton with aluminized backing	.048	.018	------	K
Kapton H (aluminized)	.041	-----	-.051	N
Mo (polished)	-----	-----	0.0	I
Nickel	.005	0.0	------	I
Ni/SiO_2	-.004	0.0	------	I
Polyurethane A-276	.023	-----	.01	L
Polyurethane A276 glossy white	.002	-----	.2	L
Polyurethane A276 with 0.5 to 1 mil OI650 overcoat	.002	-----	-.3	L
Rh foil on Al	-----	-----	0.0	N

[a]More reflective as a result of the exposed Mo substrate.
[b]Low absolute reflectance (-0.5 to 1 percent).

TABLE II. - Concluded.

Material	Change in optical properties due to atomic oxygen			Reference
	Solar absorptance	Emittance	Reflectance	
S13 - GLO	-.005	0.0	------	I
SiO_2 (650 A on Kapton H)	0.0	0.0	0.0	E
SiO_x ring	.039	-.002	------	K
Silicate MS-74	0.01	0.0	------	H,A
Silicone (black, conductive)	0.0	-.005	------	A
Silicone RTV-602/Z302	.004	-----	------	---
Silicone RTV-650+TiO_2	.001	-.01	------	A
Silicone RTV-670	-.004	-----	.001	B
Silicone S1023	-.022	-.02	------	G
Siloxane coating, RTV 602/ on aluminized Kapton, second surface mirror substrate (0.008 mm thick coating) (0.052 mm thick Kapton)	0.0	0.0	------	O
Ti/"tiodized" alloy	-----	-----	[c]-.25	N
Ti/"tiodized" CP	-----	-----	[d]-.40	N
Urethane (black, conductive)	.042	.55	------	A
Urethane inhib A-276	0.0	.01	------	A
YB-71	.004	0.0	------	I
Z302 glossy black	.043	-----	-4.3	L
Z302 with MN41-1104-0 overcoat	-.002	-----	------	M
Z302 with OI 651 overcoat	0.0	-----	------	M
Z302 with OI 650 overcoat	-.001	-----	.1	L
Z302 with RTV-602 overcoat	-.004	-----	------	L
Z302 with RTV-670 overcoat	-.004	-----	.4	L
Z306	.022	0.0	------	I
Z306 (flat black)	.028	-----	------	L
Z853, glossy yellow with MN41-1104-0 overcoat	.011	-----	------	M
Z853, yellow	-.034	-----	------	L
401 - C10 flat black	.005	-----	------	L

[c]Contrast in different spectra between STS-8 and control. Possible aging effects on controls.
[d]Aging effects similar in STS-8 and control. No exposure effect.

TABLE III. - ATOMIC OXYGEN TEST FACILITIES

Facility number	Organization	Location	Facility description	Test program participant
1	Alabama, University of	Huntsville, AL	Thermal A/O source	John Gregory
2	Auburn University	Auburn, AL	RF plasma excited N is reacted with NO gas to produce thermal ground state A/O	Charles Neely
3	Auburn University	Auburn, AL	RF plasma asher	Bruce Tatarchuk
4	Boeing Aerospace Co.	Seattle, WA	Low frequency RF plasma; samples located downstream from glow	Gary Pippin Roger Bourassa
5	Case Western Reserve University	Cleveland, OH	Variable energy ion gun	T.G. Eck Dick Hoffman
6	David Sarnoff Research Center	Princeton, NJ	Single grid, low energy ion source	Bawa Singh
7	General Electric - Space Division	Philadelphia, PA	Single grid ion source with charge exchange	Leo Amore James Lloyd
8	Jet Propulsion Lab	Pasadena, CA	Formation of O^- by dissociative attachment. Electrostatic acceleration of ions to final energy, then photodetachment of electrons from ions with a laser	Ara Chutjian Otto Orient
9	Jet Propulsion Lab	Pasadena, CA	Pulsed laser induced breakdown followed by expansion through a nozzle	David Brinza Ranty Liang
10	Lockheed Palo Alto Research	Palo Alto, CA	RF plasma asher	Matt McCargo
11	Los Alamos National Laboratory	Los Alamos, NM	Continuous laser heated discharge	Jon B. Cross
12	Martin Marietta Denver Aerospace	Denver, CO	Ion gun; magnet for charge/mass selection; multistage aperture for beam deceleration; deflection	Gary W. Sjolander
13	McDonnell Douglas Astronautics Co.	Huntington Beach, CA	RF plasma system with Faraday cage	Esther H. Lan C.A. Smith
14	NASA - Ames Research Center	Moffett Field, CA	Microwave discharge, multisample chamber	Larry L. Fewell
15	NASA - Ames Research Center	Moffett Field, CA	RF O_2 plasma; samples downstream from plasma glow	Morton Golub Ted Wydevan
16	NASA - Ames Research Center	Moffett Field, CA	RF plasma with sample downstream from glow; sample is UV shielded	Narcinda R. Lerner
17	NASA - Johnson Space Center	Houston, TX	Flowing afterglow	Steven L. Koontz
18	NASA - Johnson Space Center	Houston, TX	RF plasma asher	Steven L. Koontz
19	NASA - Langley Research Center	Hampton, VA	RP plasma asher	Carmen E. Batten
20	NASA - Langley Research Center	Hampton, VA	Electron stimulated desorption from mesh	R.A. Outlaw
21	NASA - Lewis Research Center	Cleveland, OH	Electron bombardment gridless ion source	Bruce A. Banks Sharon K. Rutledge
22	NASA - Lewis Research Center	Cleveland, OH	RF plasma asher run on air	Bruce A. Banks Sharon K. Rutledge
23	NASA - Lewis Research Center	Cleveland, OH	Dissociation and ionization in tunable microwave cavity followed by electrostatic acceleration	Dale C. Ferguson
24	NASA - Marshall Space Flight Center	MSFC, AL	Electron bombardment ion source with electromagnetic charge/mass selection downstream, then deceleration with charge neutralization and deflection of nonneutralized ions	Ralph Carruth Jill Carhorl
25	Nebraska, University of Lincoln	Lincoln, NE	RF plasma asher	John A. Woollam
26	Physical Sciences, Inc.	Andover, MA	Pulsed laser induced breakdown followed by expansion through a nozzle	George Caledonia Robert Krech

TABLE III. - CONCLUDED.

Facility number	Organization	Location	Facility description	Test program participant
27	Princeton Plasma Physics Laboratory	Princeton, NJ	Neutralization of ions formed in plasma by biased plate	William Langer S.A. Cohen D.M. Manos R.W. Motley
28	Texas, University of	Austin, TX	Ion beam with charge exchange	Dennis Kohl
29	Toronto, University of (Aerospace Institute)	Downsview, Ontario, Canada	Microwave generated plasma. Noble gas carrier transports A/O through skimmer to produce high flux density	Rod. C. Tennyson
30	Vanderbilt University	Nashville, TN	Ion gun. Wein filter for charge state selection; deceleration of ions through system of grids; grazing incidence impact with polished nickel surface to neutralize ions. Electrostatic deflection of non-neutralized ions	Royal Albridge N. Tolk
31	NASA Goodard Space Flight Center	Greenbelt, MD	RF plasma asher	Joe A. Colony Edward L. Sanford John J. Scialdone
32	University of Southampton	Highfield, Southampton, UK	Thermal arc beam facility	John Stark
33	Boeing Aerospace Co.	Seattle, WA	Negative ionization beam	Ray Rempt

TABLE IV. - COMPARISON OF ATOMIC OXYGEN TEST PROGRAM MATERIALS, PROPERTIES, AND EROSION YIELDS FROM IN-SPACE AND GROUND LABORATORY OXYGEN ION BEAM TESTS

Material	Density, gm/cm^2	Mass loss rate per area on STS-8[a] 10^{-8} gm (cm^2 sec)	Erosion yields			
			In-space tests		Ground lab ion beam tests[b]	
			Absolute yield, $10^{-24} cm^3/atom$	Relative to Kapton H	Absolute yield, $10^{-24} cm^3/atom$	Relative to Kapton HN
Kapton H or HN	1.42	1.01	3.0	1.0	23 to 46	1.0
Polyethylene	.918	.715	3.3	1.1	23 to 46	1.0
FEP Teflon	2.15	.0188	.037	.012	39 to 77	1.7
Pyrolytic graphite	2.2	.623	1.2	.40	5 to 11	.23
Highly oriented pyrolytic graphite	2.26	.640	1.2	.40	4.9 to 9.7	.21

[a]Assuming an STS-8 flux of 2.36×10^{15} atoms/(cm^2 sec) over an exposure duration of 41.17 hr to produce a fluence of 3.5×10^{20} atoms/cm^2, 4.4 to 4.5 eV atoms.
[b]Performed at an oxygen ion beam energy of 41 eV.

REFERENCES FOR TABLE I

1. Marshall Space Flight Center

2. K.A. Smith, "Evaluation of Oxygen Interaction with Materials (EOIM) - STS-8 Atomic Oxygen Effects," AIAA Paper-85-7021, Nov. 1985.

3. J.T. Durcanin, D.R. Chalmers, and J.T. Visentine, "The Definition of the Low Earth Orbital Environment and its Effect on Thermal Control Materials, AIAA Paper-87-1599, June, 1987.

4. B.A. Banks, M.J. Mirtich, S.K. Rutledge, and H.K. Nahra, in Eighteenth IEEE Photovoltaic Specialists Conference, (Institute of Electrical and Electronics Engineers, Piscataway, NJ, 1985), pp. 381-386.

5. C.K. Purvis, D.C. Ferguson, D.B. Snyder, N.T. Grier, J.V. Staskus, and J.C. Roche, "Environmental Interactions Considerations for Space Station and Solar Array Design," Dec. 1986.

6. J.T. Visentine, L.G. Leger, J.F. Kuminecz, and I.K. Spiker, "STS-8 Atomic Oxygen Effects Experiment," AIAA Paper 85-0415, Jan. 1985.

7. Langley Research Center

8. University of Alabama at Huntsville

9. D.R. Coulter, R.H. Liang, S.H. Chung, K.O. Smith, and A. Gupta, in Proceedings of the NASA Workshop on Atomic Oxygen Effects, D.E. Brinza, ed., NASA CR-181163 (NASA, Washington, D.C., 1987) pp. 39-46.

10. L.G. Leger, B. Santos-Mason, J.T. Visentine, and J. F.Kuminecz, in Proceedings of the NASA Workshop on Atomic Oxygen Effects, D.E. Brinza, ed., NASA CR-181163 (NASA, Washington, D.C., 1987) pp. 1-10.

11. British Aerospace

12. A.F. Whitaker, "LEO Atomic Oxygen Effects on Spacecraft Materials: STS-5 Results," NASA TM-86463, 1984.

14. Lewis Research Center

15. L.J. Leger, I.K. Spiker, J.F. Kuminecz, T.J. Ballentine, and J.T. Visentine, STS-T LEO Effects Experiment - Background Description and Thin Film Results," AIAA Paper 83-2631-CP, Nov. 1983.

16. Jet Propulsion Laboratory

17. J.C. Gregory, in Proceedings of the NASA Workshop on Atomic Oxygen Effects, D.E. Brinza, ed., NASA CR-181163 (NASA, Washington, D.C., 1986), pp. 29-36.

18. L.J. Leger, J.T. Visentine, and J.F. Kuminecz, "Low Earth Orbit Atomic Oxygen Effects Surfaces - of Space Shuttle Orbits," AIAA Paper 84-0548, Jan. 1984.

19. L.J. Leger, "Oxygen Atom Reaction With Shuttle Materials at Orbital Altitudes - Data and Experiment Status," AIAA Paper 83-0073, Jan. 1983.

20. Goddard Space Flight Center

21. Johnson Space Center

22. Washington University

23. W.S. Slemp, B. Santos, G.F., Sykes, Jr., and W.S. Witte, Jr., "Effects of STS-8 Atomic Oxygen Exposure on Composites, Polymeric Films and Coatings," AIAA Paper 85-0421, Jan. 1985.

24. B. Santos, "The Dependence of Atomic Oxygen Resistance on Polyimide Structures. (Preliminary results of STS-8)," NASA Headquarters, Jan. 23-24, 1984.

25. Aerospace Corporation

26. A.F. Whitaker, S.A. Little, R.J. Harwell, D.B. Griner, R.F. DeHaye, and A.T. Fromhold Jr., "Orbital Atomic Oxygen Effects on Thermal Control and Optical Materials: STS-8 Results." AIAA Paper 85-0416, Jan. 1985.

REFERENCES FOR TABLE II

A. NASA Goddard Space Flight Center

B. NASA Marshall Space Flight Center

C. NASA Langley Research Center

D. A.F. Whitaker, "LEO Atomic Oxygen Effects on Spacecraft Materials: STS-5 Results," NASA TM-86463, 1984.

E. NASA Lewis Research Center

F. NASA Langley Research Center

G. Martin Marietta

H. J.J. Park, T.R. Gull, H. Herzig, A.R. and Toft, "Effects of Atomic Oxygen on Paint and Optical Coatings."

I. W.S. Slemp, B. Santos, G.F. Sykes, Jr., and W.G. Witte, Jr., "Effects of STS-8 Atomic Oxygen Exposure on Composites, Polymeric Films, and Coatings," AIAA Paper 85-0421, Jan. 1985.

J. D.G. Zimcik, and C.R. Maag, "Results of Apparent Atomic Oxygen Reactions with Spacecraft Materials During Shuttle Flight STS-41-G," AIAA Paper 85-7020, Nov. 1985.

K. K.A. Smith, "Evaluation of Oxygen Interaction with Materials (EOIM) -STS-8 Atomic Oxygen Effects," AIAA Paper 85-7021, Nov. 1985.

L. A.F. Whitaker, S.A. Little, D.B. Harwell, R.F. Griner, R.F. DeHaye, and A.T. Fromhold, Jr., "Orbital Atomic Oxygen Effects on Thermal Control and Optical Materials: STS-8 Results," AIAA Paper 85-0416, Jan. 1985.

M. A.F. Whitaker, J.A. Burka, J.E. Coston, Z. Dalins, and S.A. Little, "Protective Coatings for Atomic Oxygen Susceptible Spacecraft Materials - STS-41G Results," AIAA Paper 85-7017, Nov. 1985.

N. M.J. Meshishnek, W.K. Stuckey, J.S. Evangelides, L.A. Feldman, R.V. Peterson, C.S. Arnold, and D.R. Peplinski, "Effects on Advanced Materials: Results of the STS-8 EOIM (Effects of Oxygen Interaction With Materials) Experiment," Report SD-TR-87-34, Aerospace Corporation, El Segundo, CA, July 20, 1987.

O. P.W. Knopf, R.J. Martin, R.E. Damman, and M. McCargo, "Correlation of Laboratory and Flight Data for the Effects of Atomic Oxygen on Polymeric Materials," AIAA Paper 85-1066, June 1985.

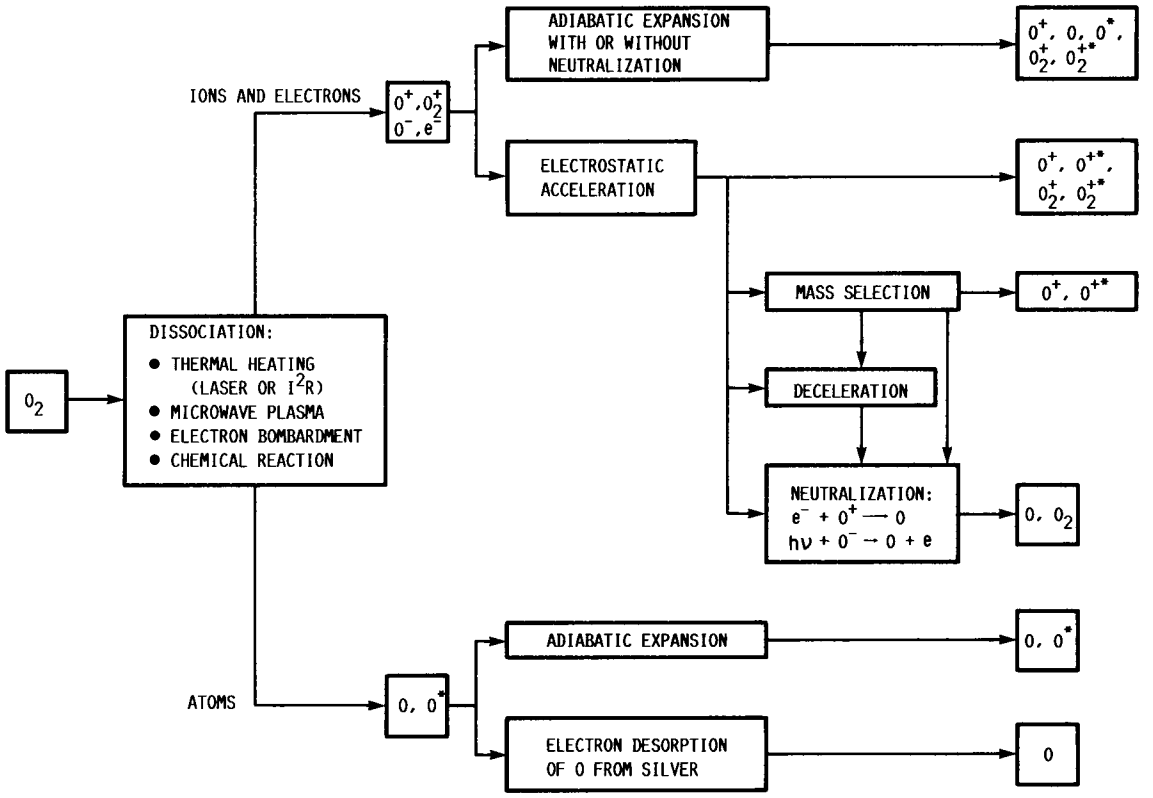

FIGURE 1. - PROCESSES USED FOR SIMULATION OF LOW EARTH ORBITAL ATOMIC OXYGEN.

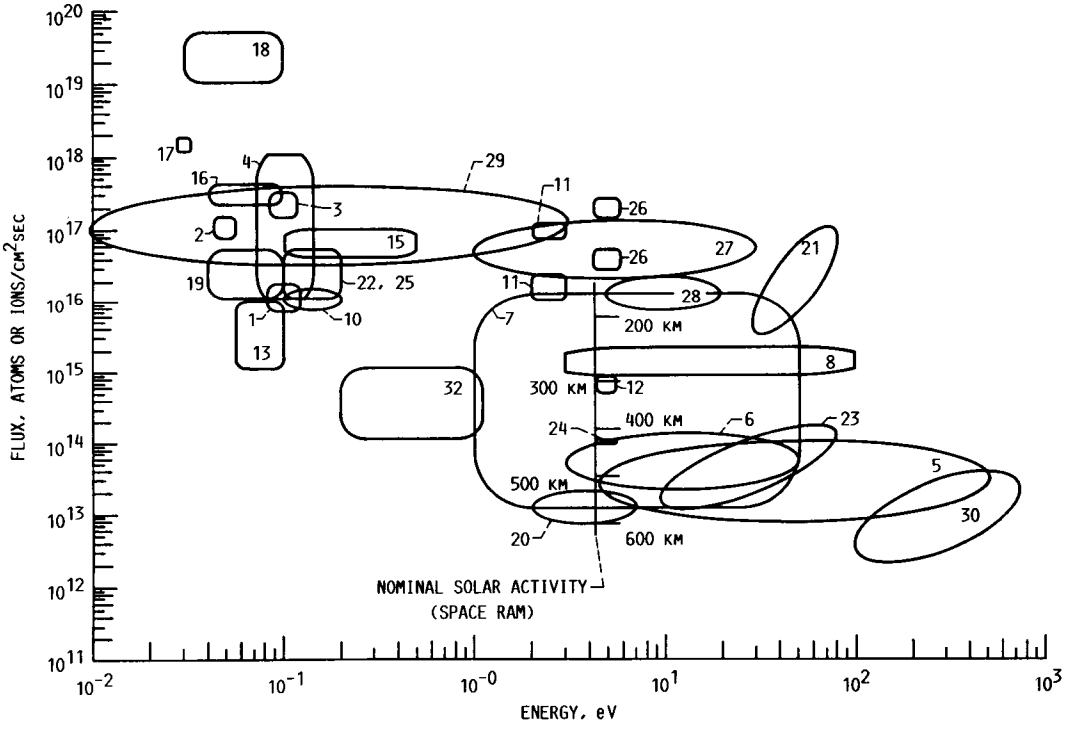

FIGURE 2. - ATOMIC OXYGEN TEST FACILITY FLUX ENERGY DOMAINS.

ORIGINAL PAGE IS
OF POOR QUALITY

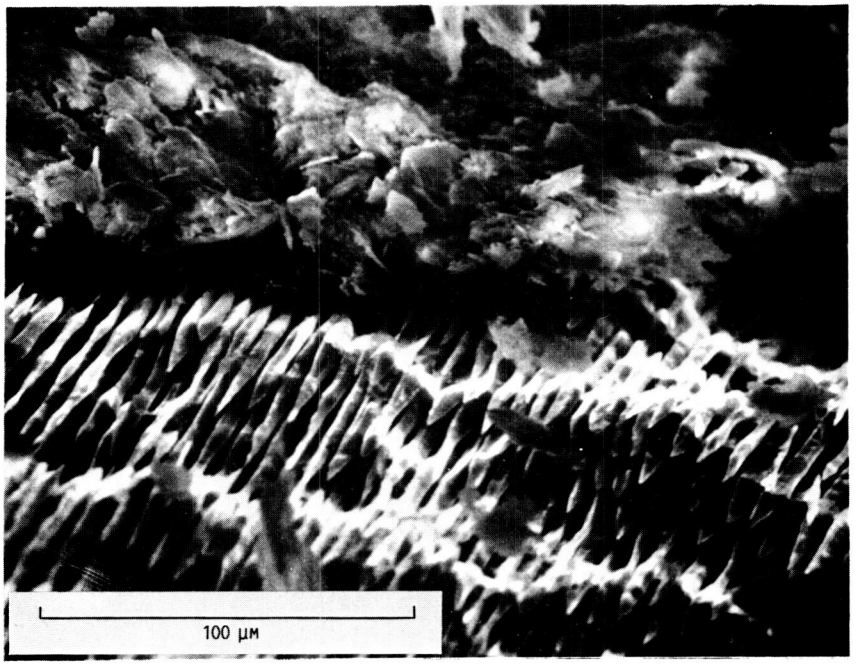

FIGURE 3. - 20.6 MASS PERCENT MICA PAINT ON GRAPHITE EPOXY AFTER 228 HOURS OF EXPOSURE IN AN ASHER. BOTTOM PORTION SHOWS UNDERLYING GRAPHITE EPOXY SUBSTRATE AFTER MICA FLAKES HAVE BEEN REMOVED.

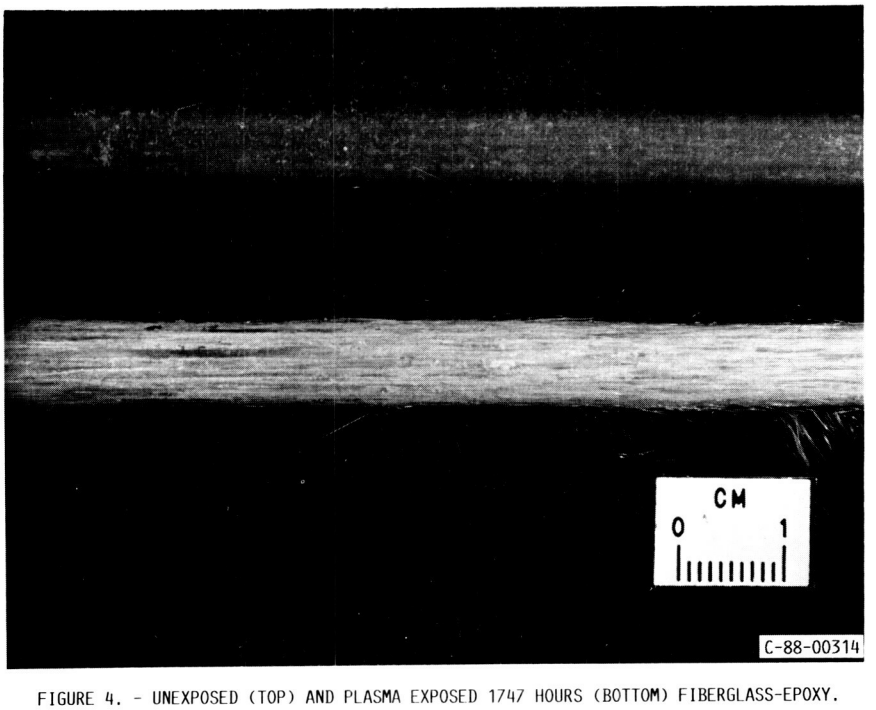

FIGURE 4. - UNEXPOSED (TOP) AND PLASMA EXPOSED 1747 HOURS (BOTTOM) FIBERGLASS-EPOXY.

ORIGINAL PAGE IS
OF POOR QUALITY

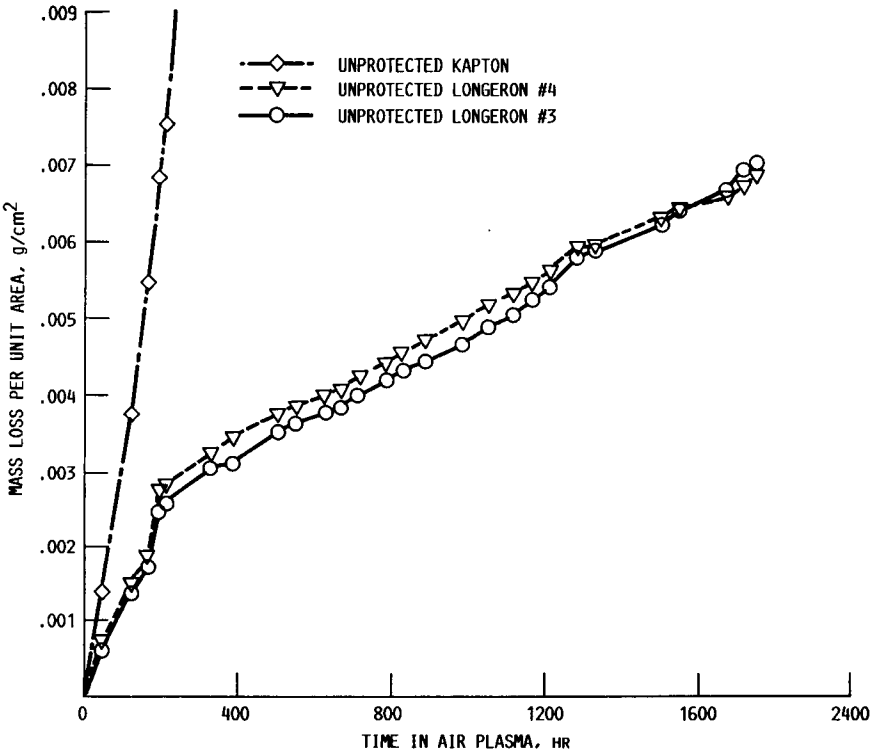

FIGURE 5. - MASS LOSS VERSUS PLASMA EXPOSURE TIME FOR UNPROTECTED FIBERGLASS EPOXY.

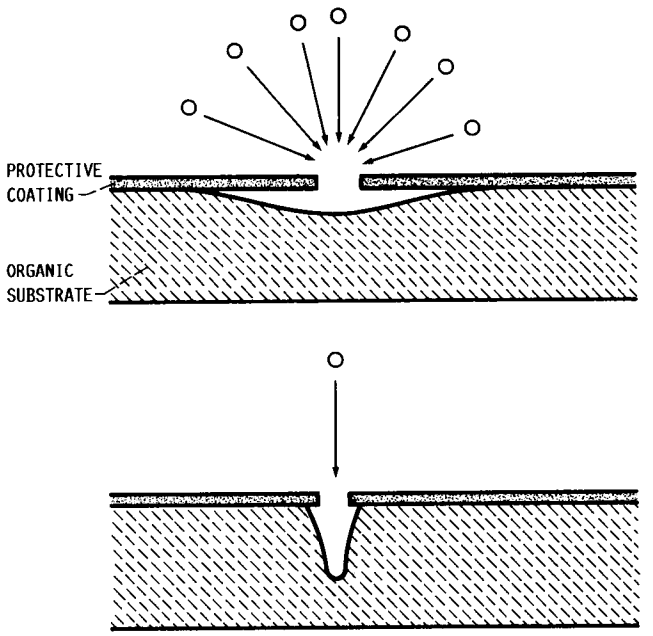

FIGURE 6. - POTENTIAL DIFFERENCE IN ATOMIC OXYGEN UNDERCUTTING BETWEEN RF PLASMA ASHER EXPOSURE (TOP) AND IN-SPACE EXPOSURE (BOTTOM).

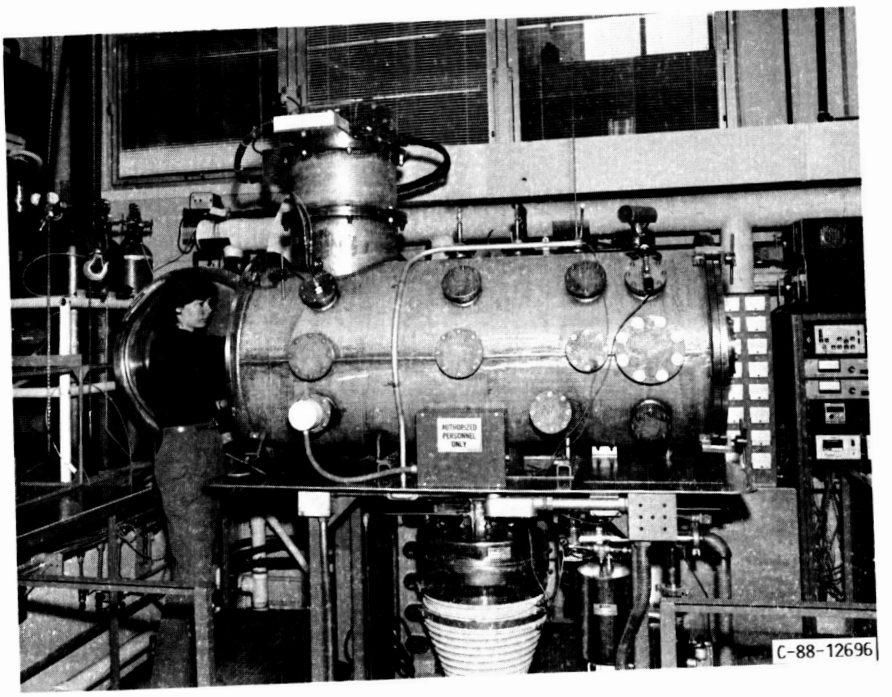

FIGURE 7. - OXYGEN ION BEAM FACILITY.

ORIGINAL PAGE IS
OF POOR QUALITY

ORIGINAL PAGE IS
OF POOR QUALITY

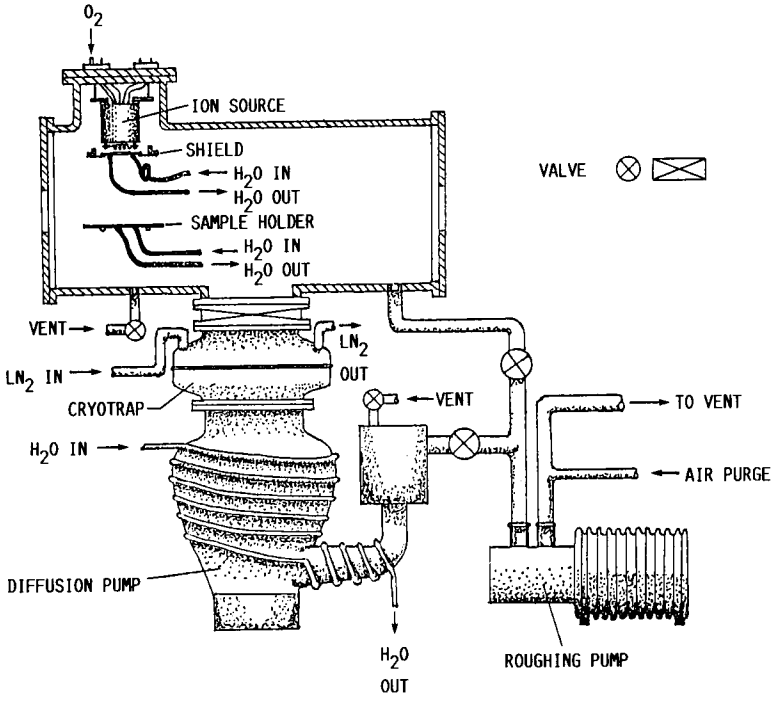

FIGURE 8. - SCHEMATIC OF OXYGEN ION BEAM VACUUM SYSTEM.

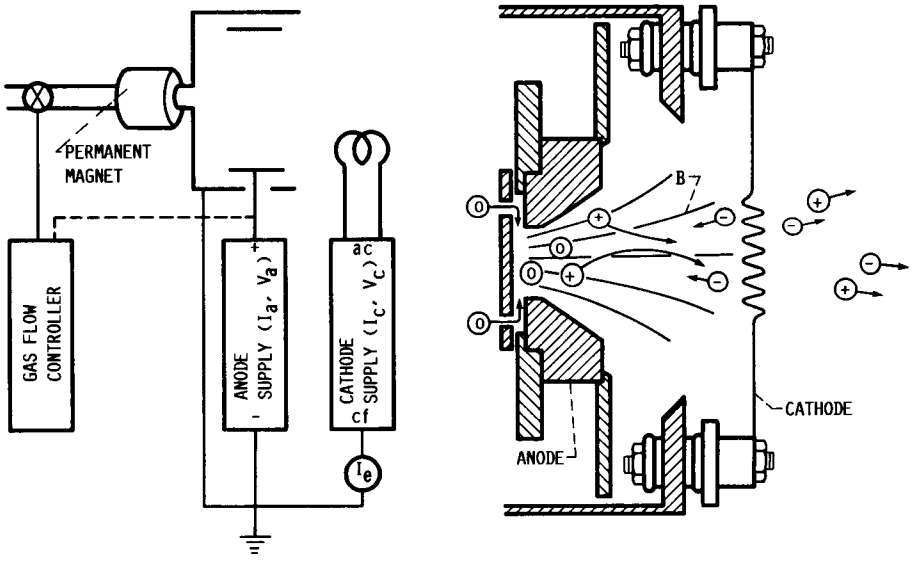

FIGURE 9. - GRIDLESS ION SOURCE.

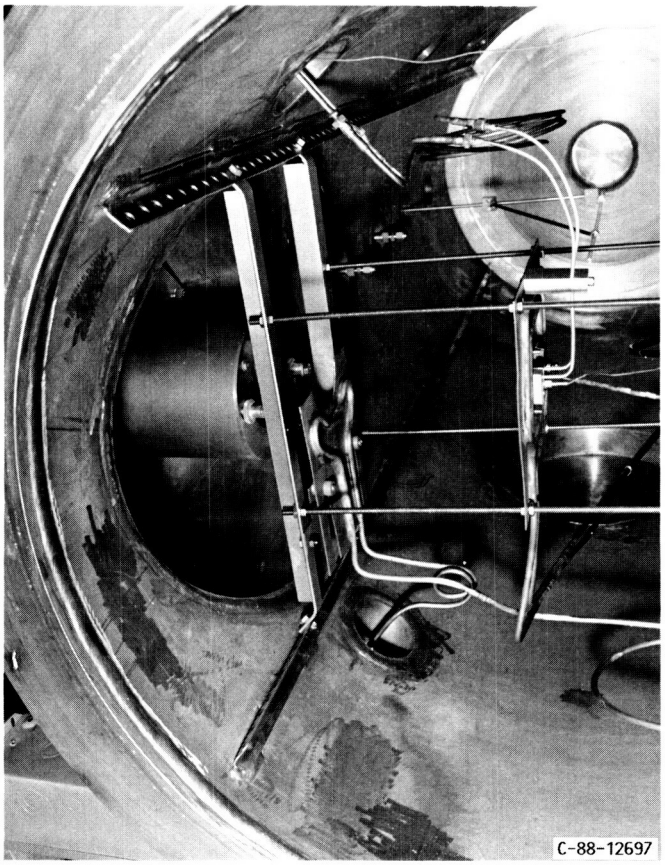

(A) LOOKING UP TOWARD THE ION SOURCE.

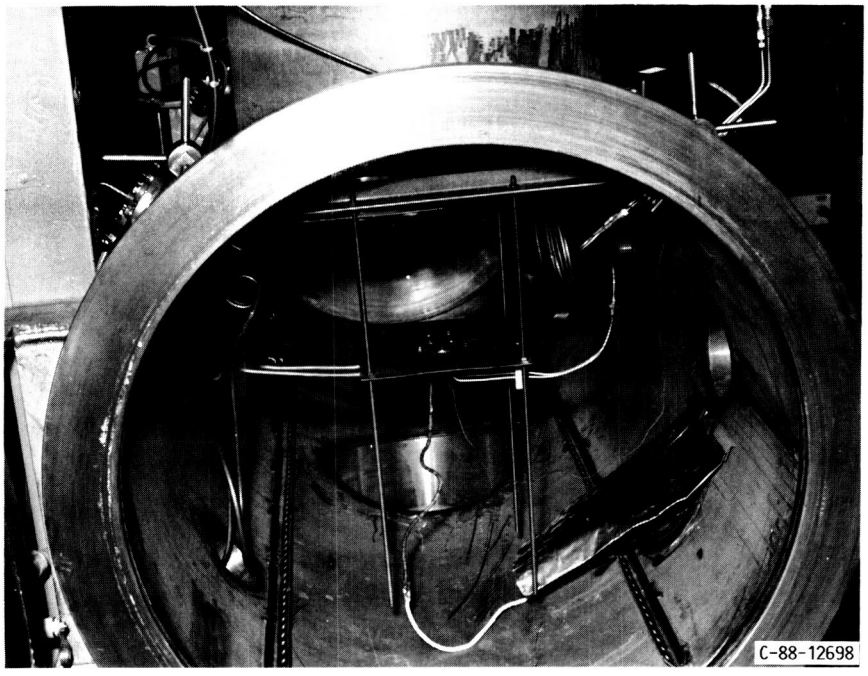

(B) LOOKING DOWN TOWARD THE SAMPLE HOLDER PLATE.

FIGURE 10. - PHOTOGRAPHS OF GRIDLESS ION SOURCE IN RELATION TO THE SAMPLE HOLDER PLATE.

ORIGINAL PAGE IS
OF POOR QUALITY

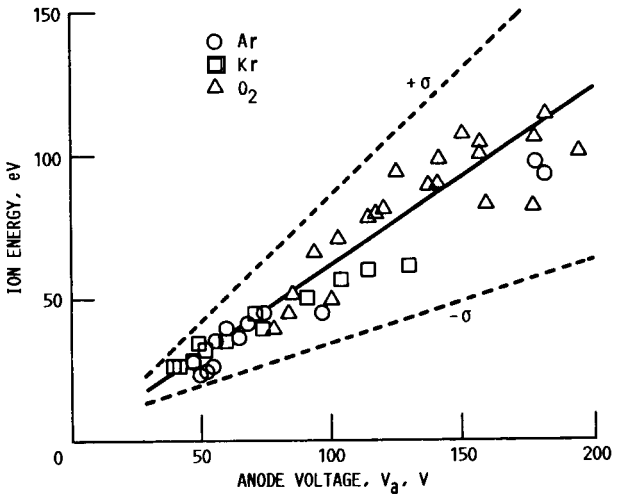

FIGURE 11. - ION ENERGY DEPENDENCE UPON ION SOURCE DISCHARGE VOLTAGE.

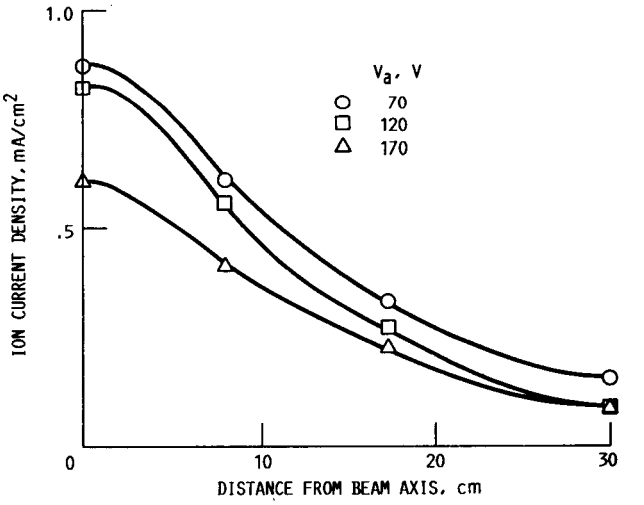

FIGURE 12. - CURRENT DENSITY PROFILES AT AN ANODE CURRENT OF 5 A, AND A SOURCE TARGET DISTANCE OF 30 cm, USING OXYGEN. FLAT TARGET NORMAL TO BEAM AXIS.

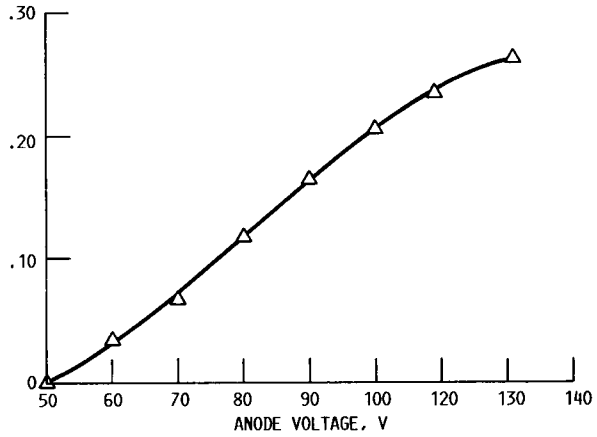

(A) AS A FUNCTION OF ANODE VOLTAGE.

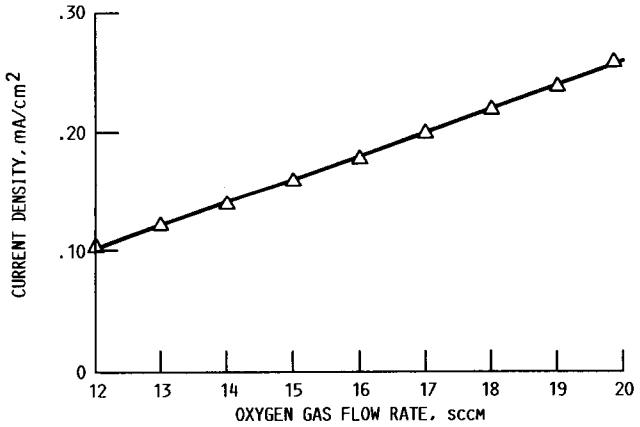

(B) AS A FUNCTION OF OXYGEN FLOW RATE.

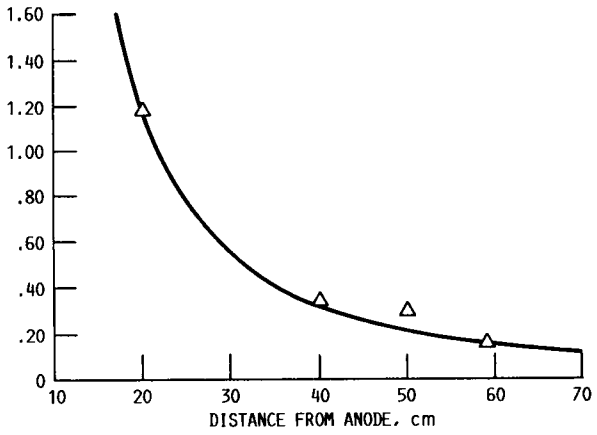

(C) AS A FUNCTION OF AXIAL DISTANCE DOWNSTREAM OF THE ION SOURCE.

FIGURE 13. - OXYGEN ION CURRENT DENSITY.

ORIGINAL PAGE IS
OF POOR QUALITY

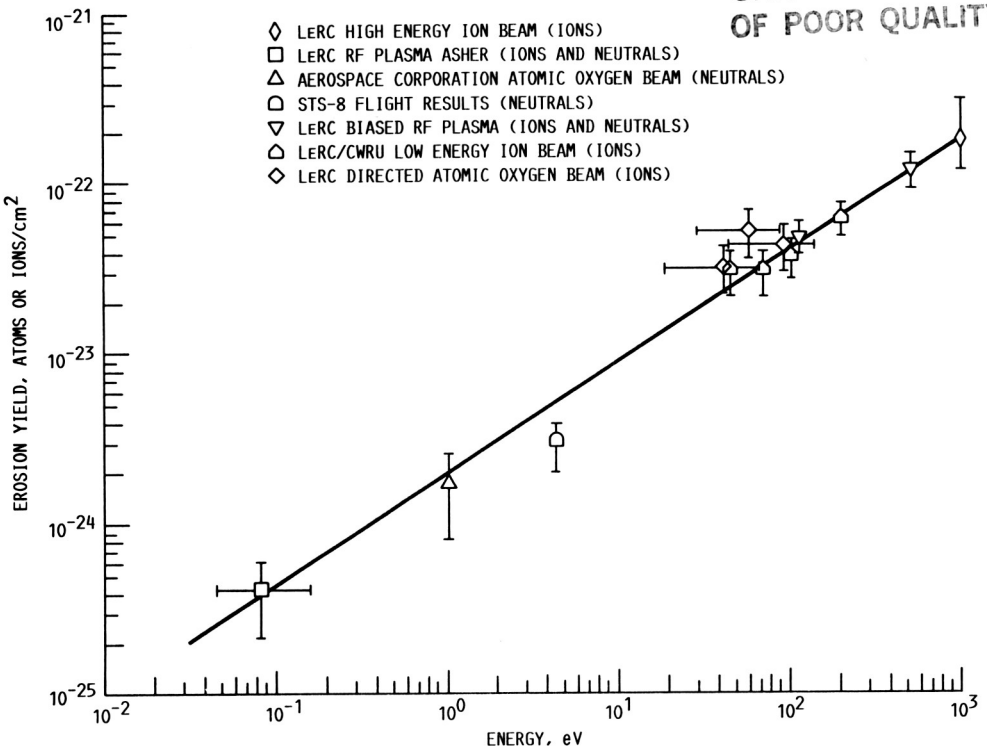

FIGURE 14. - EROSION YIELD DEPENDENCE OF KAPTON POLYIMIDE AS A FUNCTION OF OXYGEN ION OR ATOM ENERGY.

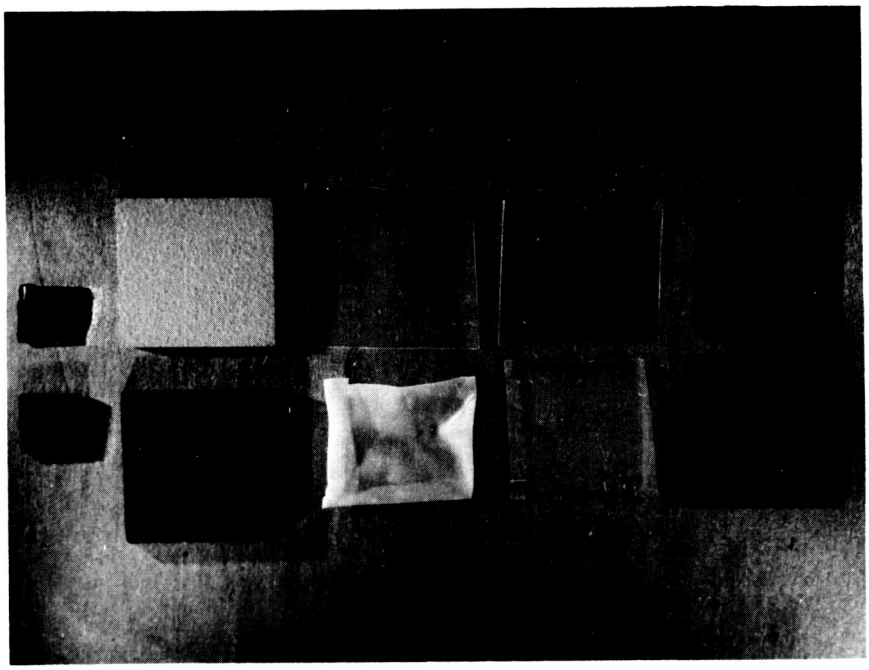

FIGURE 15. - PHOTOGRAPH OF KAPTON HN, POLYETHYLENE, FEP TEFLON, PYROLYTIC GRAPHITE, AND HIGHLY ORIENTED PYROLYTIC GRAPHITE BEFORE AND AFTER ION BEAM EXPOSURE TO A FLUENCE OF 7×10^{18} TO 1.5×10^{19} ATOMS/cm^2.

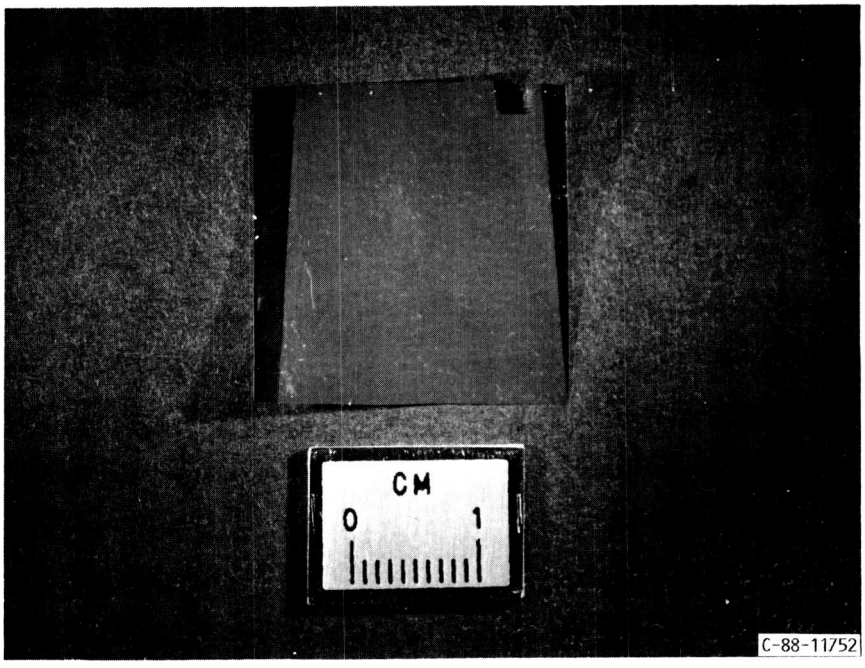

FIGURE 16. - KAPTON HN EXPOSED TO AN OXYGEN ION BEAM TO A FLUENCE OF 3×10^{19} TO 6×10^{19} ATOMS/cm^2 SHOWING CLEAR SPECULAR TRANSMITTANCE ON AREA OF THE SAMPLE PROTECTED FROM ION BEAM EXPOSURE AND DIFFUSE REFLECTANCE ON AREAS OF THE SAMPLE EXPOSED TO THE ION BEAM.

ORIGINAL PAGE IS
OF POOR QUALITY

ORIGINAL PAGE IS
OF POOR QUALITY

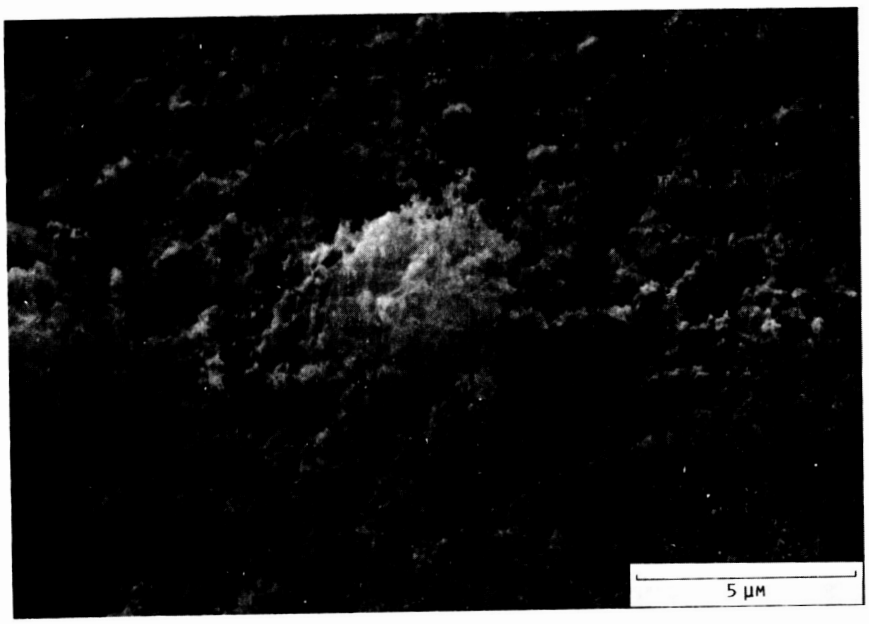

(A) KAPTON HN AFTER 3 x 10^{19} TO 6 x 10^{19} ATOMS/cm^2.

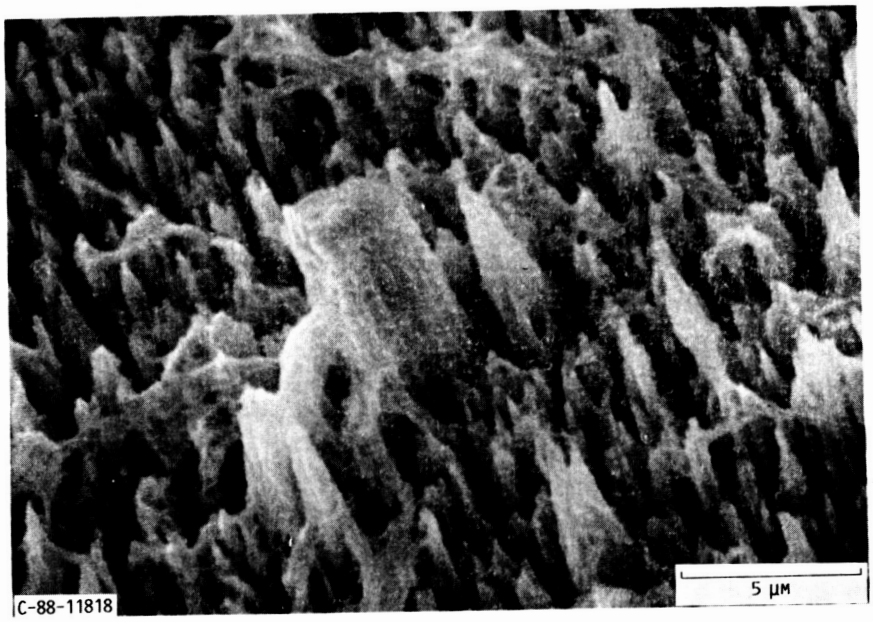

(B) PRYOLYTIC GRAPHITE AFTER 8 x 10^{19} TO 1.6 x 10^{20} ATOMS/cm^2.

FIGURE 17. - SCANNING ELECTRON PHOTOMICROGRAPHS OF THE SURFACE OF MATERIALS EXPOSED TO AN OXYGEN ION BEAM.

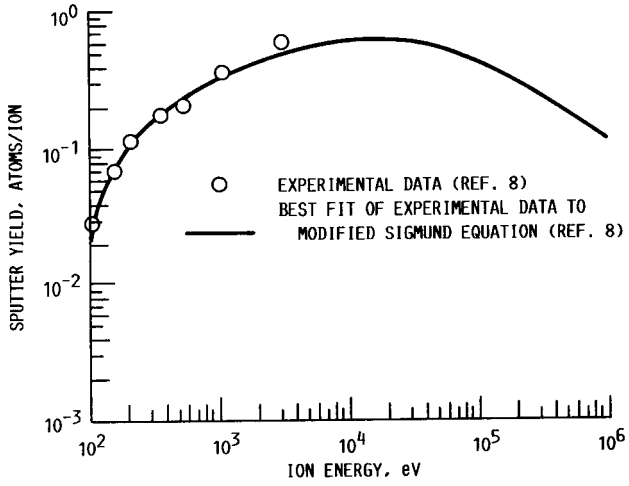

FIGURE 18. - SPUTTER YIELD OF NICKEL VERSUS OXYGEN ION ENERGY.

NASA
National Aeronautics and Space Administration

Report Documentation Page

1. Report No.	2. Government Accession No.	3. Recipient's Catalog No.
NASA TM-101971		

4. Title and Subtitle	5. Report Date
Simulation of the Low Earth Orbital Atomic Oxygen Interaction With Materials by Means of an Oxygen Ion Beam	6. Performing Organization Code

7. Author(s)	8. Performing Organization Report No.
Bruce A. Banks, Sharon K. Rutledge, Phillip E. Paulsen, and Thomas J. Steuber	E-4671
	10. Work Unit No. 506-43-11

9. Performing Organization Name and Address	11. Contract or Grant No.
National Aeronautics and Space Administration Lewis Research Center Cleveland, Ohio 44135-3191	13. Type of Report and Period Covered Technical Memorandum

12. Sponsoring Agency Name and Address	14. Sponsoring Agency Code
National Aeronautics and Space Administration Washington, D.C. 20546-0001	

15. Supplementary Notes

Prepared for the 18th Annual Symposium on Applied Vacuum Science and Technology, sponsored by the American Vacuum Society, Clearwater, Florida, February 6-8, 1989. Bruce A. Banks and Sharon K. Rutledge, NASA Lewis Research Center; Phillip E. Paulsen, Cleveland State University, Dept. of Electrical Engineering, Cleveland, Ohio 44115; Thomas J. Steuber, Sverdrup Technology, Inc., NASA Lewis Research Center Group, Cleveland, Ohio 44135.

16. Abstract

Atomic oxygen is the predominant species in low-Earth orbit between the altitudes of 180 and 650 km. These highly reactive atoms are a result of photodissociation of diatomic oxygen molecules from solar photons having a wavelength less than or equal to 2430 Å. Spacecraft in low-Earth orbit collide with atomic oxygen in the 3P ground state at impact energies of approximately 4.2 to 4.5 eV. As a consequence, organic materials previously used for high altitude geosynchronous spacecraft are severely oxidized in the low-Earth orbital environment. The evaluation of materials durability to atomic oxygen requires ground simulation of this environment to cost effectively screen materials for durability. Directed broad beam oxygen sources are necessary to evaluate potential spacecraft materials performance before and after exposure to the simulated low-Earth orbital environment. This paper presents a description of a low energy, broad oxygen ion beam source used to simulate the low-Earth orbital atomic oxygen environment. The results of materials interaction with this beam and comparision with actual in-space tests of the same materials will be discussed. Resulting surface morphologies appear to closely replicate those observed in space tests.

17. Key Words (Suggested by Author(s))	18. Distribution Statement
Atomic oxygen Low Earth Orbit Oxygen ion beam	Unclassified - Unlimited Subject Category 27

19. Security Classif. (of this report)	20. Security Classif. (of this page)	21. No of pages	22. Price*
Unclassified	Unclassified	32	A03

NASA FORM 1626 OCT 86

*For sale by the National Technical Information Service, Springfield, Virginia 22161